ESE 498 Capstone Design Project:

Convolutional Neural Network for 2-D MRI Image Reconstruction in k-space

Submitted to Professors Wang and the Department of Electrical and Systems Engineering

Date Submitted: August 3, 2023
Conducted: December 2022 – August 2023

Kerri Prinos
Department of Electrical and Systems Engineering
B.S./M.S. Electrical Engineering
k.prinos@wustl.edu

Advisors:

Dr. Ulugbek Kamilov
Computational Imaging Group
Department of Electrical and Systems Engineering, Department of Computer Science and Engineering
kamilov@wustl.edu

Yuyang Hu (Ph.D. candidate)
Computational Imaging Group
Department of Electrical and Systems Engineering

ABSTRACT

Deep learning algorithms, such as convolutional neural networks (CNNs), are powerful tools for accelerating brain magnetic resonance imaging (MRI) image reconstruction, greatly improving the imaging process for patients and healthcare workers. We use the U-net architecture – a CNN architecture – to reconstruct: (1) a 2-D MRI brain image from a zero-filled image in the image domain and (2) a 2-D MRI brain image from a zero-filled image in k-space. We use images from the Brain Dataset from Aggarwal et al. [1-2] to train and evaluate our model. We assess the quality of the reconstructed images from each task using average PSNR and SSIM. Image reconstruction in the image domain yielded an average PSNR and SSIM values of 27.50 dB and 0.7855, respectively. For image reconstruction in k-space, we obtained an average PSNR value of 28.59 dB and an average SSIM of 0.7050.

INTRODUCTION

Magnetic Resonance Imaging (MRI) is a valuable, non-invasive diagnostic tool in medicine. Brain MRI is advantageous over other imaging methods since it does not expose the patient to radiation, and it provides high-resolution images of the brain and surrounding tissues [3-5]. This is essential for monitoring and diagnosing diseases and disorders that affect the brain [3-5]. The downside to brain MRI is the lengthy acquisition time. A brain MRI can take anywhere from 30–90 minutes to complete, which makes MRI difficult to use in time-sensitive situations, as in the case of a stroke [5-6]. Motion artifacts from patient movement reduce image quality, so infants, patients with Parkinson's disease or claustrophobia often require general anesthesia for long scans, which poses its own risks [7-9]. While decreasing acquisition times improves patient comfort and reduces medical cost, it leads to severe degradation of image quality [8-9].

Image Domain and k-space

Raw MRI data is collected in k-space as an array of frequency- and phase-encoded spatial information [10]. Fig. 1 illustrates the relationship between the image domain and k-space. The image of the brain on the left is the result of the inverse Fourier transform of the k-space data. In the k-space representation on the right in Fig. 1, each pixel represents a spatial frequency [6, 10]. The center of the k-space array contains the low spatial frequency components and the edges contain the high spatial frequency components [6, 10].
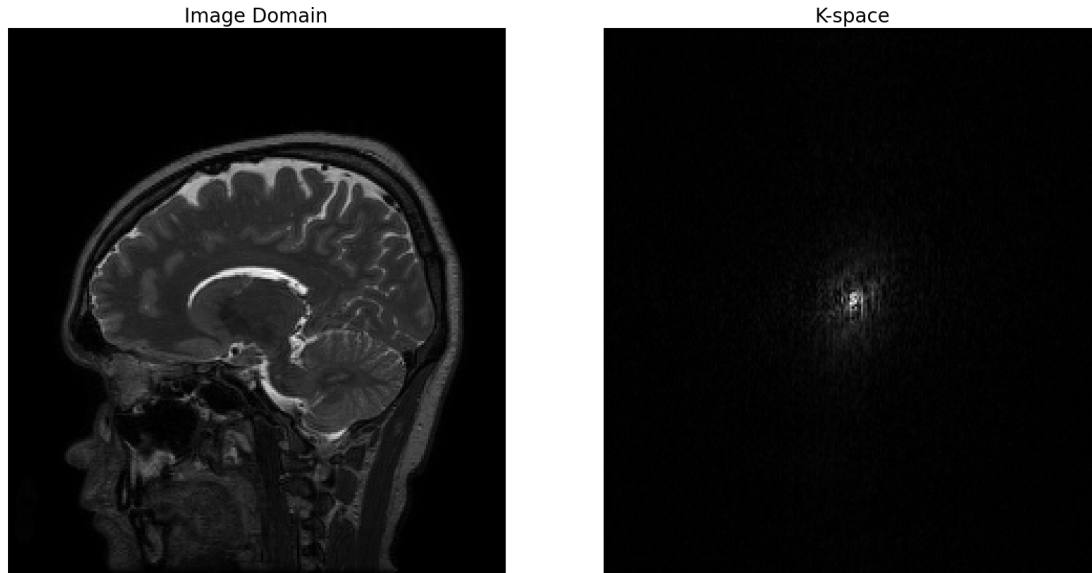
Figure 1. *Left:* A fully sampled brain MRI image in the image domain.
Right: The same image in k-space (the Fourier transform of the image domain).
Images obtained from the dataset [1-2].

MRI acquisition can be accelerated by undersampling in k-space [6, 11]. For example, by acquiring only one-sixth of the data points, you can achieve 6-fold acceleration [11]. The missing data points are filled in with 0's, a process known as zero-filling. Zhu et al. [12] found that zero-filling reduces the patchwork effect that appears at the pixel-level. From this, concluded that zero-filling is always necessary in order to visualize structures – but not artifacts – in high resolution as illustrated by Figure 2 [12].
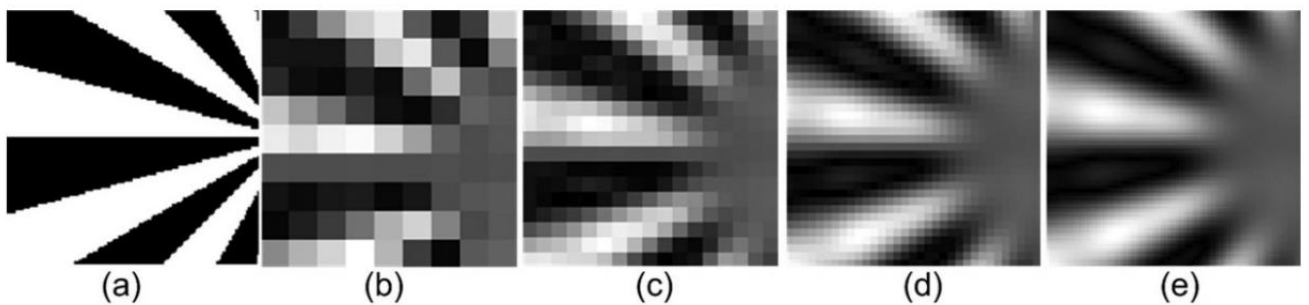

Figure 2. Zhu et al. use part of the Siemens star resolution phantom to demonstrate the necessity of zero-filling for visualizing structures in high resolution. The zero-fill factors increase from left to right (b-e) resulting in a higher resolution image and less pixelation artifacts. The image with the highest zero-fill factor (e) most closely resembles the original image (a) [12, Fig. 4]
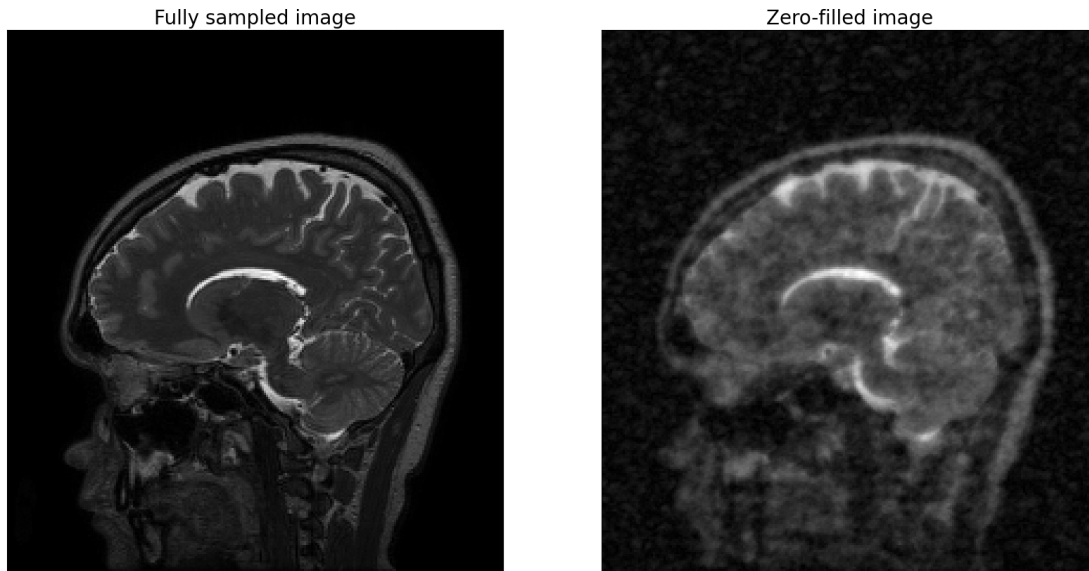
Figure 3. *Left:* A fully sampled brain MRI image
Right: A zero-filled image created using a random undersampling mask to do 6-fold acceleration. Images obtained from the dataset [1-2].

Even so, zero-filled images are more distorted and contain more aliasing artifacts than fully-sampled images, as seen in Figure 3 [6]. Previous works have demonstrated that deep-learning based methods, such as convolutional neural networks (CNNs), are one of the most powerful tools for reconstructing MRI images from zero-filled images in both the image domain [8] and directly in k-space [13].

Convolutional Neural Networks

CNNs are a type of deep learning algorithm that is used for image classification and object recognition tasks [14]. There is a feedforward process for feature extraction and classification and a backward path for training [14]. Fig. 4 illustrates typical CNN architecture for feedforward computation, which has three main types of layers: a convolutional layer, a pooling or subsampling layer, and a fully-connected layer [14].
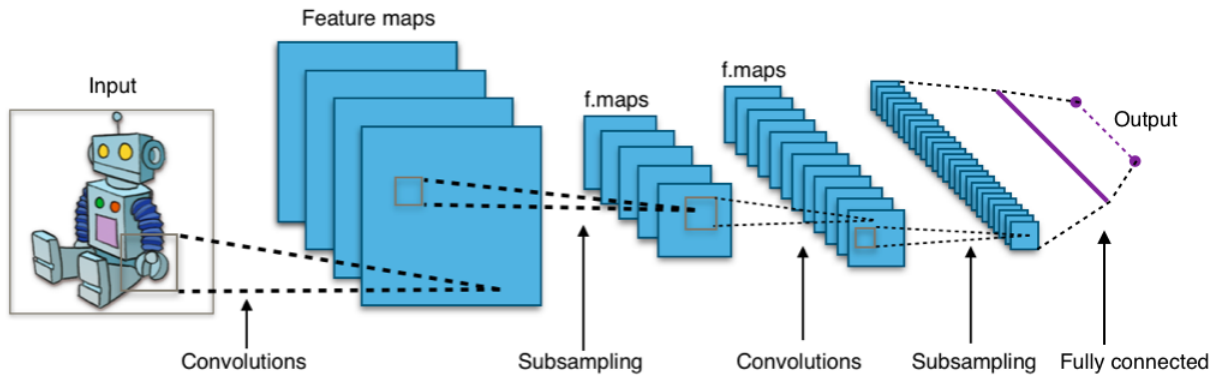
Figure 4. Overview of typical CNN architecture for feedforward computation [15]. Note the three main types of layers: a convolutional layer, a pooling or subsampling layer, and a fully connected layer. Feature maps are the result of the convolution of the input image and the feature detectors.

The feature maps are the result of the convolution of the input image and the feature detectors [14]. In Fig. 4, these feature detectors detect simple features, such as the outline of the robot or the different colors [14-15]. As the image progresses through the layers of CNN architectures, the layers become more complex [14-15]. For example, in Fig. 4, the network will recognize small groups of features, such as the edges and color of the robot's antenna or feet. Then it will identify larger elements, such as the head or torso, and eventually, it identifies the entire figure as a robot.

U-net Architecture for MRI image reconstruction

The U-net architecture is a convolutional network architecture that was developed by Ronneberger et al. [16] for biomedical segmentation applications. Ronneberger et al. [16] presented a U-net architecture consisting of two paths: a contracting path (left side) and an expansive path (right side), which gives it the characteristic U-shape as seen in Fig. 5 [16, Fig. 1].
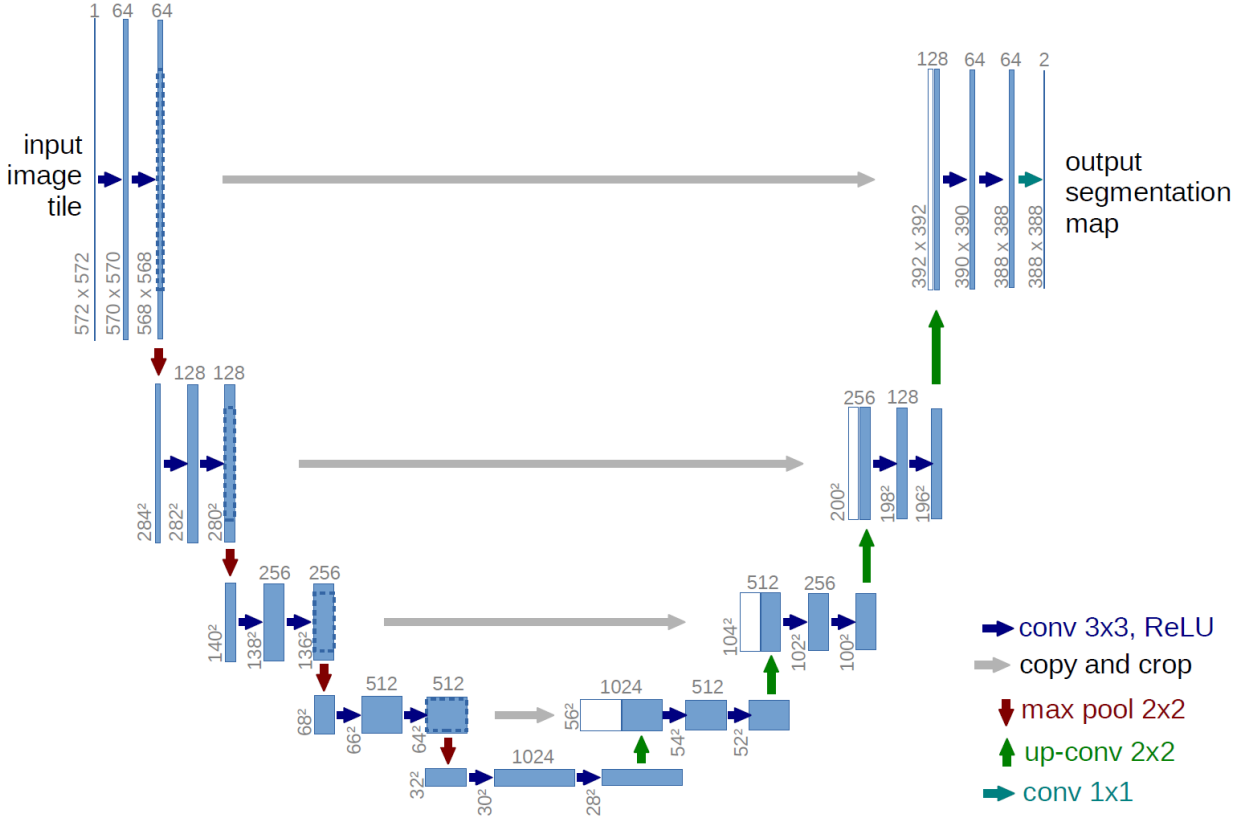
Figure 5. The original U-net architecture for biomedical image segmentation developed by Ronneberger et al. [16, Fig. 1]. Each blue box represents a multi-channel feature map. The number of channels are listed at the top of these boxes, and the x-y dimensions are listed to the side of the boxes. The two channels at the start and end are for the real and imaginary components of the data. The legend explains the color coded arrows that show convolution, max pool, and copy and crop operations.

The contracting path is similar to the example architecture of Fig. 4. Fig. 5 illustrates the sequence of the following operations: 3 x 3 unpadded convolutions, a rectified linear unit (ReLU) that helps the network to converge, and 2 x 2 max pooling operations with stride 2 for downsampling [16]. Ronneberger et al. [16] include a copy and crop operation after each set of two convolutions due to the loss of border pixels in every convolution. The final layer uses a 1x1 convolution to map the 64-component feature vector to the number of desired segmentation classes [16].

Jin et al. [8] first adapted the U-net architecture to perform image reconstruction tasks. Their modifications include the use of zero-padding to prevent the image size from decreasing with each convolution and replacing the last layer with a convolutional layer that reduces the 64-component feature vector to one output image [8]. Jin et al. [8] also replace the copy and crop operation with a copy and concatenate operation to improve model convergence in backpropagation [17]. The U-net model is effective for image reconstruction because the many

convolutions in both paths result in high-level local and global feature recognition [10,13,20]. Since its introduction for MRI image reconstruction, many researchers have achieved better results by modifying the basic U-net architecture [1, 6-9,11,17-24]. Our objectives are to reconstruct: (1) a 2-D MRI brain image from a zero-filled image in the image domain and (2) a 2-D MRI brain image from a zero-filled image in k-space. Du et al. theorized that training CNNs in k-space to interpolate the missing k-space data points will achieve better performance than training in the image domain [13, 22]. We aim to support this theory with the eventual goal of performing 3-D reconstruction directly in k-space. We will be using the basic U-net architecture for our image reconstruction tasks, as it provides a baseline for comparing our results to those in existing literature.

METHODS

MRI reconstruction can be described by an inverse problem. In (1), we define the inverse problem that recovers a ground truth image $\mathbf{x} \in \mathbb{C}^n$ from a noisy measurement $\mathbf{y} \in \mathbb{C}^n$ characterized by the linear model:

$$\mathbf{y} = \mathbf{PFx} + \mathbf{e},\qquad\qquad (1)$$

where $\mathbf{F} \in \mathbb{C}^{n \times n}$ denotes the Fourier transform, $\mathbf{P} \in \mathbb{F}^{n \times n}$ is a sampling operator, and $\mathbf{e} \in \mathbb{C}^{n \times n}$ is a noise vector. Both arrays are random undersampling masks to do 6-fold acceleration. The zero-filled images are given by:

$$\hat{\mathbf{x}}_i = \{\mathbf{F}^{-1}\mathbf{y}_i\}_i^N\qquad\qquad (2)$$

where $\mathbf{F}^{-1}$ denotes the inverse Fourier transform and N is the total number of training samples.

2-D Reconstruction

For 2-D reconstruction, we used the Brain Dataset from Aggarwal et al. [1-2]. The parallel MRI brain data of five human subjects was collected using 3D T2 CUBE sequences with Cartesian readouts using a 12-channel head coil. The dataset includes an array called tnrOrg, which contains the fully sampled MRI data in the image domain from four test subjects. trnOrg is a complex array with dimensions 256 x 232 x 360. There are 90 slices from each of the four subjects, and each slice is of spatial dimension 256 x 232.

trnOrg served as our ground truth $\{\mathbf{x}\}_i^N$ in the image domain. For our ground truth in k-space, we used the Fourier transform of the trnOrg. We also used trnMask from the dataset, which is a random undersampling mask to do 6-fold acceleration. We used (1) to find the noisy measurement with trnMask as $\mathbf{P}$. y was our zero-filled image in k-space. We applied (2) to find the zero-filled images in the image domain. We trained the CNN f_θ by mapping zero-filled images (2) to their desired ground truth $\{\mathbf{x}\}_i^N$ in both the image domain and k-space. We used a 80-10-10% split for the training, testing, and validation datasets.

All our code was written in Python 3.10.11 on Google Colab. We used the NVIDIA T4 TensorCore GPUs available on Google Colab for training and testing our model. Since we chose to use Pytorch version 2.0.1 optimized with CUDA version 11.8, we could easily use the

PyTorch implementation of a U-net model from Zbontar et al. [16, 21]. We instantiated the U-net model as follows:

```
# setting up unet model, loss function, and optimizer
model = Unet(in_chans=2,
        out_chans=2,
        chans = 32,
        num_pool_layers = 4,
        drop_prob  = 0.0)
```

We used two channels to handle the real and imaginary components of the MRI data as in [24], and a batch size of 16. Figure 6 provides a detailed, visual representation of the U-net architecture.
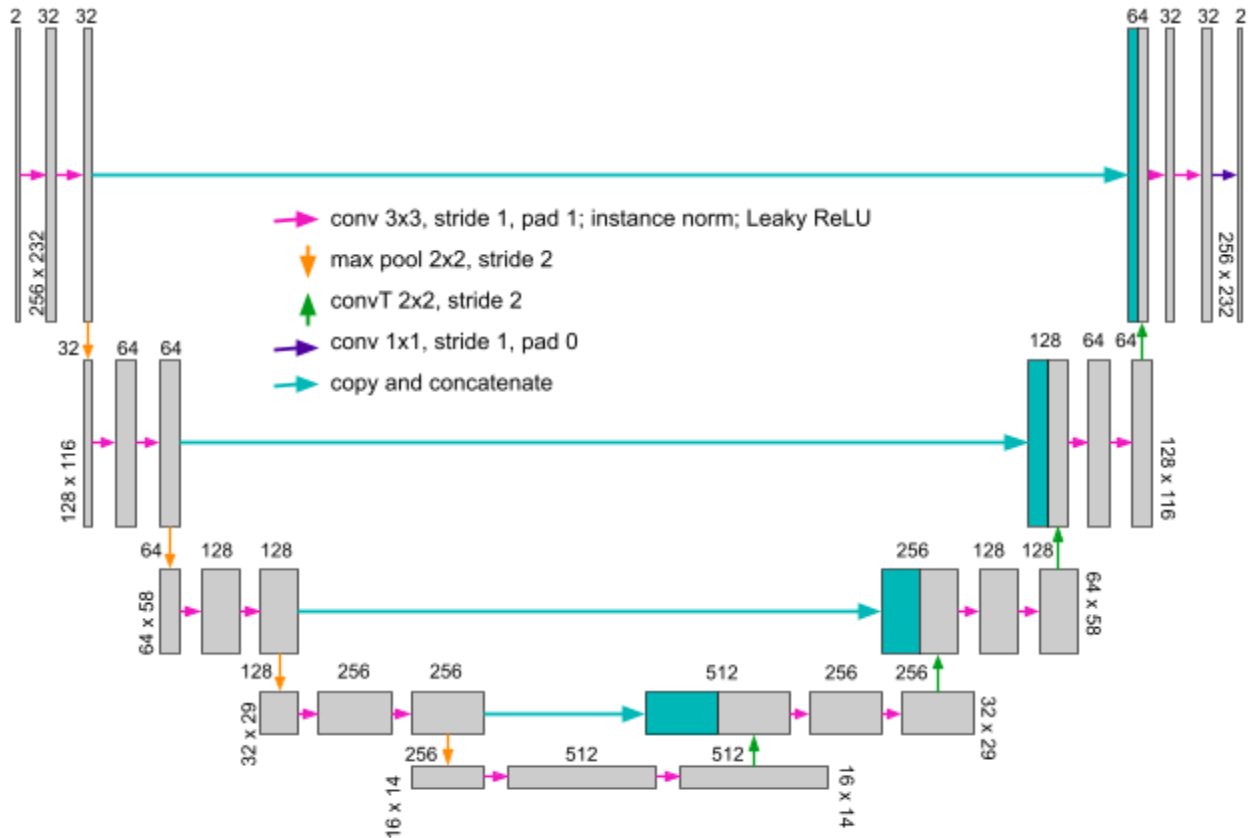

Figure 6. U-net architecture for 2-D reconstruction. The gray boxes represent multi-channel feature maps and the teal boxes represent the copied feature maps. The number of channels are listed at the top of these boxes, and the x-y dimensions are listed to the side of the boxes. The two channels at the start and end are for the real and imaginary components of the data. The

legend explains the color coded arrows that show convolution, max pool, and copy and concatenate operations. This figure was adapted from: [8 Fig. 2; 16, Fig. 1; 21, Fig. 7;].

This U-net model has 7,756,418 parameters, which are all trainable parameters. For 2-D reconstruction in the image domain, the network was trained for 200 epochs with Adam optimization, a learning rate of 0.0001, and the mean squared error (MSE) loss function defined in (3).

$$\mathcal{L}_{\mathrm{MSE}}(\hat{\mathbf{x}}, \mathbf{x}) = \frac{1}{N} \sum_{i}^{N} \| f_\theta(\hat{\mathbf{x}}_i) - \mathbf{x}_i \|_2^2$$

(3)

Achieving desirable image quality was more challenging in k-space. The network was trained for 200 epochs, and we compared the results of different combinations of optimizers, learning rates, loss functions. We also compared the effect of normalization on the training dataset. The array X of raw data in k-space was normalized as follows:

```python
# Normalization of images in k-space
for i in range(X.shape[0]):
  X[i] /= np.amax(np.abs(X[i]))
```

In addition to the Adam optimizer and MSE loss function, we also tried the RMSprop optimizer and L1 loss function (4) as in Zbontar et al. [21]. We tried various learning rates from 0.0001 to 0.01.

$$\mathcal{L}_{\mathrm{L1}}(\hat{\mathbf{x}}, \mathbf{x}) = \frac{1}{N} \sum_{i=1}^{N} |\hat{x}_i - x_i|$$

(4)

DATA TO BE COLLECTED AND PROCEDURE FOR ACQUIRING

For both reconstruction tasks, we will be evaluating the performance using qualitative and quantitative metrics. An arbitrary image will be selected from ground truth from the testing set for a side by side comparison with its zero-filled image and reconstructed image. We will use the average peak signal-to-noise ratio (PSNR) and the average structural similarity index measure (SSIM) of the testing set to quantitatively assess the quality of the reconstructed image. SSIM and PSNR are widely used in MRI reconstruction research, so it will be beneficial to compare our values to those in literature.

We use the psnr() and ssim() functions from the metrics model from scikit-image, which is an open-source library for image processing in Python, to calculate the average PSNR and SSIM for the reconstructed test images. As the name suggests, the PSNR is the ratio of the maximum signal in the ground truth image to the mean-square error between the reconstructed and ground truth images. The PSNR in decibels can be calculated as in (5):

$$\mathrm{PSNR}(x, \hat{x}) = 10 \log_{10} \left(\frac{\mathrm{MAX}^2}{\frac{1}{N} \sum_{i=1}^{N} (x_i - \hat{x}_i)^2} \right), \quad (5)$$

where x is the ground truth image, $\hat{x}$ is the reconstructed image, MAX represents the maximum signal in the ground truth image, and N is the total number of pixels in the ground truth image. A higher PSNR value of 30-50 dB indicates better image reconstruction. Wang et al. developed the SSIM index to complement simpler metrics such as PSNR [27]. SSIM "compares local patterns of pixel intensities that have been normalized for luminance and contrast," so it better aligns with the way humans perceive image quality. The Structural Similarity Index (SSIM) between x and $\hat{x}$ is given by (6):

$$\mathrm{SSIM}(x, \hat{x}) = \frac{2\mu_x \mu_{\hat{x}} + C_1}{\mu_x^2 + \mu_{\hat{x}}^2 + C_1} \cdot \frac{2\sigma_{x\hat{x}} + C_2}{\sigma_x^2 + \sigma_{\hat{x}}^2 + C_2} \cdot \frac{\sigma_{x\hat{x}}}{\sigma_x \sigma_{\hat{x}} + C_3}, \quad (6)$$

where μ_x and $\mu_{\hat{x}}$ represent the means of x and $\hat{x}$, respectively. σ_x and $\sigma_{\hat{x}}$ denote the standard deviations, and $\sigma_{x\hat{x}}$ represents the covariance between x and $\hat{x}$. C_1, C_2, and C_3 are small constants for numerical stability. SSIM values range from 0 to 1. We want an SSIM value close to 1, which indicates that the reconstructed image is very similar to the ground truth image.

RESULTS

Using the U-net model, we were able to reconstruct 2-D MRI images in both the image domain and in k-space.

2-D Reconstruction in the Image Domain

The first task served as an effective feasibility study. We used the PyTorch implementation of a U-net model from Zbontar et al. [21] to map the 2-D zero-filled MRI images in the image domain to their desired ground truth images, also in the image domain [16, 21]. The model was trained over 200 epochs using the MSE loss function and the Adam optimization algorithm with a learning rate of 0.0001. The duration of the training process was approximately 25 minutes and used 5.6 GB of GPU RAM.

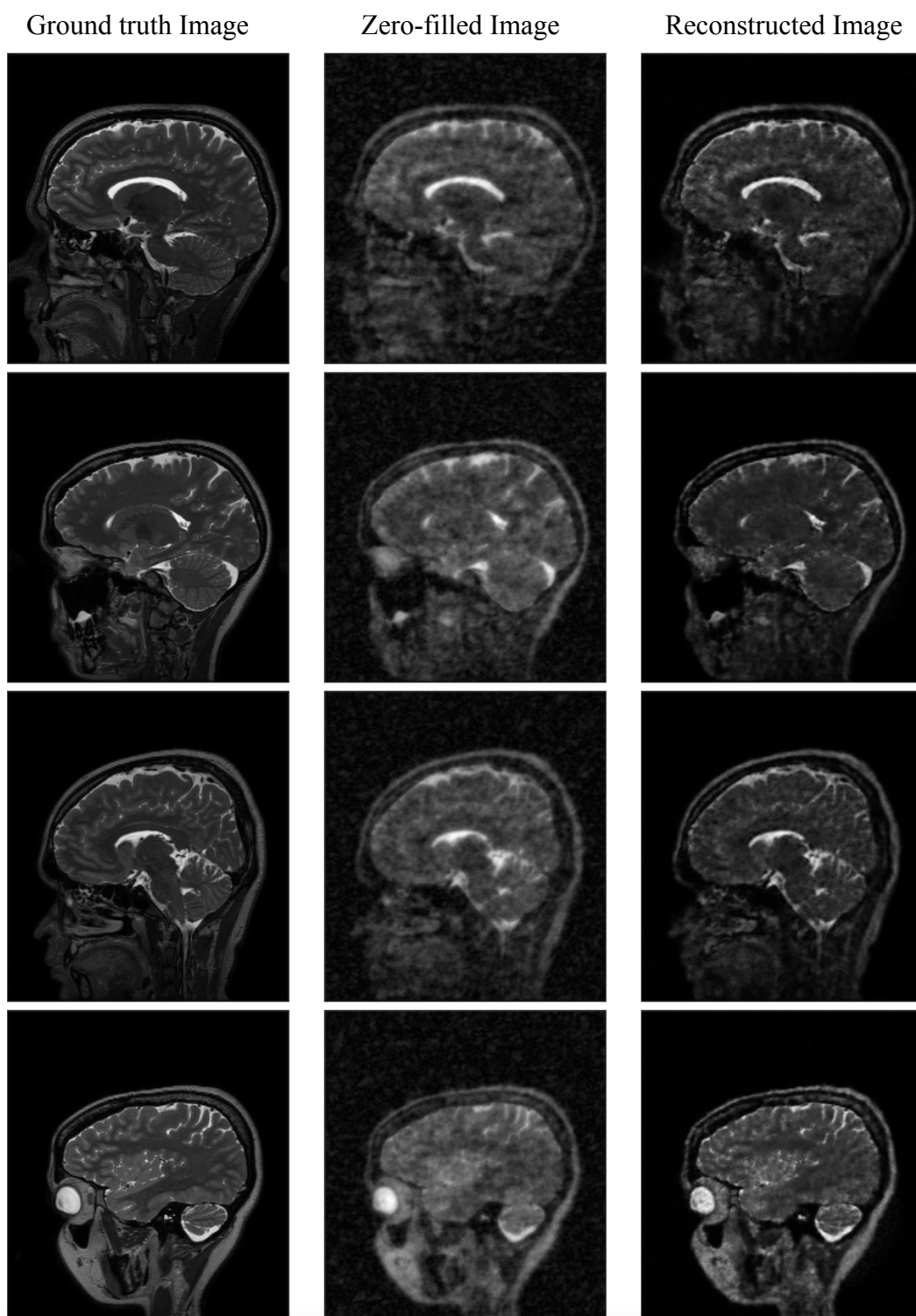Ground truth Image   Zero-filled Image   Reconstructed Image

Figure 7. Side by side comparisons of the ground truth images from the testing set (left) and their corresponding zero-filled images (middle), and reconstructed images (right). Reconstruction was performed in the image domain. Images are from the dataset [1-2].

Figure 7 shows a qualitative comparison of a randomly selected ground truth image from the testing set and its corresponding zero-filled image and reconstructed image. Note, the brain tissue can be seen in more detail in the reconstructed image compared to the zero-filled image. This observation is reflected in the PSNR and SSIM values, as well. Quantitatively comparing a randomly selected reconstructed image to its corresponding ground truth image, we obtained an average PSNR value of 27.50 dB and an average SSIM value of 0.7855. Both these values show significant improvement over the average PSNR value of 24.77 dB and the average SSIM value of 0.4860 for the corresponding zero-filled image compared to the ground truth image.

2-D Reconstruction in *k*-space

For 2-D reconstruction in k-space, we trained the model over 200 epochs. We compared the effects of combinations of various loss functions, optimizers, learning rates and with or without raw data normalization.

Table 1. Comparison of CNN models for 2-D reconstruction in k-space. The average PSNR and SSIM values in green show improvement over 24.77 dB and 0.4860 – the average PSNR and SSIM for the zero-filled images compared to the ground truth images. Those in red show a decline in image quality compared to the zero-filled images.

Model	Raw Data Normalization?	Loss Function	Optimizer	Learning Rate	Average PSNR (dB)	Average SSIM
1	No	MSE	Adam	0.0001	19.98	0.2236
2	Yes	MSE	Adam	0.0001	17.37	0.4512
3	No	MSE	RMSprop	0.01	27.76	0.5724
4	No	L1	RMSprop	0.01	24.98	0.5481
5	No	MSE	Adam	0.01	28.59	0.7050
6	Yes	MSE	Adam	0.01	24.04	0.4071

As seen in Table 1, model 5 achieved the best quality reconstructed image as indicated by the high average PSNR and SSIM values of 28.59 dB and 0.7050, respectively. Figure 8 shows a qualitative comparison of a randomly selected ground truth image from the testing set and its corresponding zero-filled image and reconstructed image.

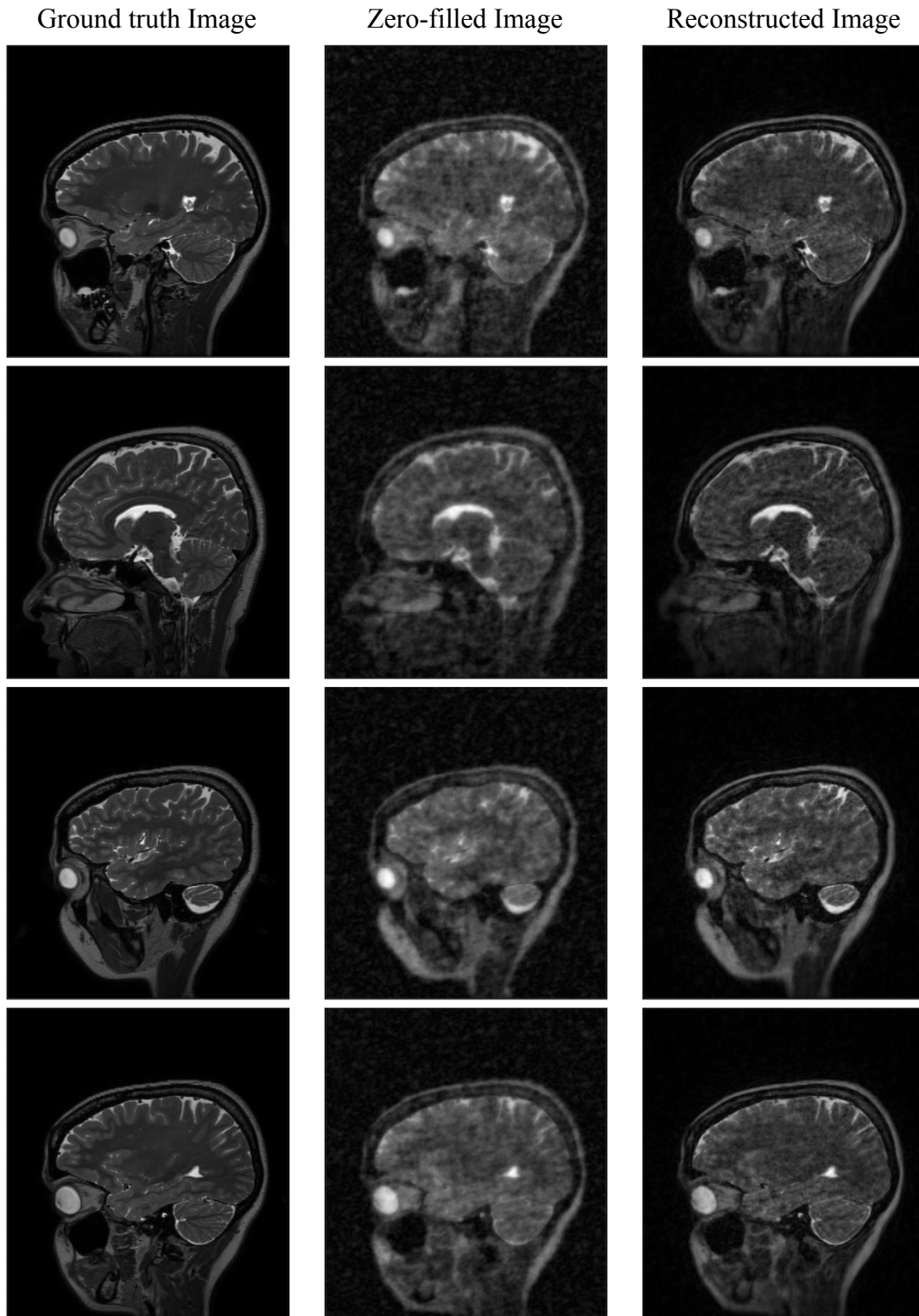Ground truth Image   Zero-filled Image   Reconstructed Image

Figure 8. Side by side comparisons of the ground truth images from the testing set (left) and their corresponding zero-filled images (middle), and reconstructed images (right). Reconstruction was performed in k-space. Images are from the dataset [1-2].

In model 5, there was no normalization of the raw data, and we trained it over 200 epochs with the MSE loss function and the Adam optimization algorithm with a learning rate of 0.01. The duration of the training process was approximately 25 minutes and used 5.6 GB of GPU RAM. The average PSNR of 28.59 dB for k-space reconstruction has a 1.09 dB or 3.96% improvement over the average PSNR for image domain reconstruction. The average SSIM value of 0.7050 has a 0.0805 or 10.25% decline compared to the average SSIM for image domain reconstruction.

DISCUSSION

Our objectives are to use the U-net architecture – a CNN architecture – to reconstruct: (1) a 2-D MRI brain image from a zero-filled image in the image domain and (2) a 2-D MRI brain image from a zero-filled image in k-space. We also aim to demonstrate that reconstruction in k-space will achieve better performance than reconstruction in the image domain.

For the first reconstruction task in the image domain, we obtained an average PSNR of 27.50 dB and an average SSIM value of 0.7855. For the second reconstruction task in *k*-space, we obtained an average PSNR of 28.59 dB and an average SSIM value of 0.7050. Both of these values show significant improvement over the average PSNR and SSIM values of 24.77 dB and 0.4860, respectively for the corresponding zero-filled image compared to the ground truth image. Both the qualitative (Fig. 7-8) and quantitative improvements in reconstructed image quality over the zero-filled images demonstrate our success in the reconstruction tasks. Additionally, the PSNR and SSIM values for the reconstructed images in the image domain [6, 7, 9, 11, 21] and k-space [1, 6-9, 11, 18, 20-24] are comparable to those in the literature for reconstruction using basic U-Net models.

Completing the second task is a great achievement, as 2-D reconstruction in k-space has not been completed by our lab previously. The 1.09 dB or 3.96% improvement in average PSNR for k-space reconstruction compared to image domain reconstruction supports the theory that training in k-space achieves better performance than training in the image domain [13, 22]. Since background noise can reduce the SSIM, we are not as concerned about the decline in average SSIM in the k-space reconstruction compared to the image domain reconstruction. However, this should be further examined in future studies.

There are limitations to the image quality that can be achieved with the basic U-net model. Our next step will be to incorporate the model for k-space reconstruction designed here into another framework for improvement. The *regularization by artifact-removal (RARE)* image reconstruction framework introduced by Liu et al. in [28] shows great promise for high quality 3-D image reconstruction from heavily undersampled k-space measurements in the image domain. With our model for k-space reconstruction and a few modifications to the gradient descent steps, we can adapt RARE for k-space reconstruction to greatly improve the quality of our 2-D reconstructed images [28-29]. Ultimately, we aim to perform 3-D reconstruction directly in k-space. Sandino et al. [17] extended the work of Jin et al. using the U-net architecture for 3-D cardiac MRI images. Instead of directly inputting the 3-D data into the

U-net model, Sandino et al. [17] separated the 3-D volume into a series of 2-D slices to be input into the model.

Future studies could combine our work with that of Sandino et al. [17] and Liu et al. [28], to perform direct k-space interpolation for 3-D MRI images of the brain. That is, we want to perform deep learning with RARE on heavily undersampled 3-D images without breaking them into 2-D slices as done in previous works [17, 28]. The inverse problem posed in (1) is also valid for 3-D image reconstruction in k-space [7]. Our 2-D U-net architecture can be changed to a 3-D U-net architecture. The operations in the 2-D U-net architecture in Fig. 5 would be changed from their 2-D to their 3-D versions, ex. 3-D instead of 2-D convolutions. Then, we would input the 3-D images in k-space, splitting real and imaginary components into two channels as before, and obtain the 3-D reconstructions also in k-space.

CONCLUSIONS

Our work demonstrates the effectiveness of a simple U-net architecture – a CNN architecture – for 2-D brain MRI image reconstruction in both the image domain and in k-space. Qualitative and quantitative measurements illustrate the quality of the reconstructed images. In the image domain, the average PSNR and SSIM values of the reconstructed image were 27.50 dB and 0.7855. In k-space, the average PSNR and SSIM values of the reconstructed image were 28.59 dB and 0.7050. The improvement in average PSNR for the image reconstructed in k-space compared to in the image domain is significant. Our results support the need to continue to develop deep learning methods for interpolation in k-space to accelerate brain MRI without sacrificing image quality. These images were reconstructed from zero-filled images created using a random undersampling mask to do a 6-fold acceleration. Such an acceleration will improve patient comfort and reduce medical cost.

DELIVERABLES

The deliverables of this project include:
- The **Python code** for training the convolutional neural network in both the image domain and in k-space. We also include Python code for the proposed 3-D U-net architecture.
- The **average PSNR and SSIM values**, which provide a quantitative measure of success for each task.
- The **reconstructed brain MRI images**, which provide a qualitative measure of success for each task.
- A **web page** explaining the project and presenting the above deliverables.
- A **final report and poster presentation** providing an in-depth explanation of the project, the methods, and the results achieved for each task.

TIMELINE FOR PROJECT COMPLETION

The Gantt chart (Fig. 9) illustrates the initial project schedule, including deadlines for the steps required to complete the deliverables. Table 2 details each task.

Table 2. Tasks to be completed and project schedule

	Task	Duration (days)	Start	Finish	Predecessors
1	Formal proposal	NA*	1/31/23	6/1/23	
2	Improving & fixing errors in task 2 code	18	6/1/23	6/18/23	
3	Update report with task 2 results	3	6/19/23	6/21/23	2
4	Research and testing for task 3	18	6/22/23	7/9/23	2,3
5	Improving & fixing errors in task 3 code	6	7/10/23	7/15/23	4
6	Update report with task 3 results	3	7/16/23	7/18/23	5
7	Final report draft	4	7/19/23	7/23/23	6
8	Final report update based on feedback	7	7/24/23	7/30/23	7
9	Final presentation	7	7/24/23	7/30/23	7
10	Final webpage	7	7/24/23	7/30/23	7

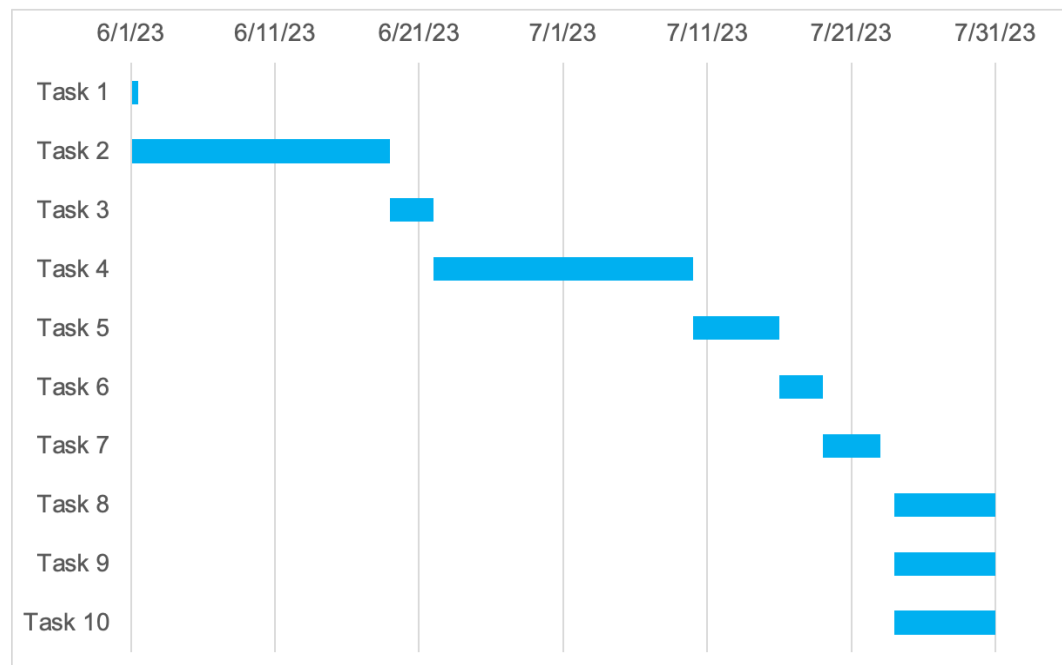* progress interrupted due to medical condition

Figure 9. Gantt chart for anticipated timeline for project completion.

Following the interruption in progress due to a medical condition during the months of February to June, we mostly adhered to the outlined schedule above. Task 2 was completed on schedule. However, once we began to work on Task 3, it became clear that we would not have time to delve into 3-D reconstruction in the time that remained. We began working to modify the RARE method from [28] to perform in k-space. It took a couple of weeks to research and understand this method and the changes to be made. Unfortunately, we were unable to use the modified code for training data due to GPU and runtime constraints on Google Colab. Our colleague had success running the original code on PyCharm, but we were unable to access PyCharm for use on this project in the time we had. These modifications to the RARE method were important as they will enable future testing for 2-D reconstruction in k-space using our U-net model as well as testing for 3-D reconstruction directly in k-space using our proposed 3-D model. The completion of the final report, website, and poster were only delayed 4 days.

REFERENCES

[1]   H.K. Aggarwal, M.P. Mani, and M. Jacob, "MoDL: Model Based Deep Learning Architecture for Inverse Problems," 2019. [Online serial]. Available: https://arxiv.org/abs/1712.02862. [Accessed Feb. 7, 2023].

[2]   H.K. Aggarwal, M.P. Mani, and M. Jacob, "Brain Dataset," *Github: hkaggarwal/modl*, 2019. Available: https://drive.google.com/file/d/1qp-l9kJbRfQU1W5wCjOQZi7I3T6jwA37/view. [Accessed Dec. 2, 2022].

[3]   Mayo Clinic Staff, "MRI." Mayo Clinic. https://www.mayoclinic.org/tests-procedures/mri/about/pac-20384768. [Accessed May 30, 2023].

[4]   Mount Sinai, "Head MRI." Mount Sinai. https://www.mountsinai.org/health-library/tests/head-mri. [Accessed May 30, 2023].

[5]   Cleveland Clinic, "Brain MRI." Cleveland Clinic. https://my.clevelandclinic.org/health/diagnostics/22966-brain-mri. [Accessed May 30, 2023].

[6]   M.B. Hossain, K.-C Kwon, R.K. Shinde, S.M. Imtiaz, and N. Kim, "A Hybrid Residual Attention Convolutional Neural Network for Compressed Sensing Magnetic Resonance Imaging Reconstruction," *Diagnostics*, vol. 13, no. 7, pp. 1306, 2023. [Online]. Available: MDPI, https://www.mdpi.com. [Accessed May 15, 2023].

[7]   Z. Ramzi, P. Ciuciu, and J. Starck, "Benchmarking MRI Reconstruction Neural Networks on Large Public Datasets, *Appl Sci*, vol. 10, no. 2, pp.1816, 2020. [Online]. Available: MDPI, https://www.mdpi.com. [Accessed May 15, 2023].

[8]   K.H. Jin, M.T. McCann, E. Froustey, and M. Unser, "Deep Convolutional Neural Network for Inverse Problems in Imaging," *IEEE Transactions on Image Processing*, vol. 26, no.9, pp. 4509-4522, 2017. [Online]. Available IEEE Xplore, https://ieeexplore.ieee.org/Xplore/home.jsp. [Accessed May 14, 2023].

[9]   C.M. Hyun, H.P. Kim, S.M. Lee, S. Lee, and J.K. Seo, "Deep learning for undersampled MRI reconstruction," *Physics in Medicine and Biology*, vol. 63, no.13, pp. 135007, 2018. [Online]. Available: IOPScience, https://iopscience.iop.org. [Accessed May 14, 2023].

[10]   T.A. Gallagher, A.J. Nemeth, and L. Hacein-Bey, "An Introduction to the Fourier Transform: Relationship to MRI," *American Journal of Roentgenology*, vol. 190, no. 5, 2008. [Online]. Available: American Journal of Roentgenology, https://www.ajronline.org. [Accessed May 30, 2023].

[11]   T. Rahman, "Fast Magnetic Resonance Image Reconstruction With Deep Learning Using An Efficientnet Encoder," 2021. [Online serial]. Available: https://scholarworks.utep.edu/cgi/viewcontent.cgi?article=4323&context=open_etd. [Accessed Feb. 7, 2023].

[12]   X. Zhu, B. Tomanek, and J. Sharp, "A Pixel is an Artifact: On the Necessity of Zero-Filling in Fourier Imaging," *Concepts Magn Reson*, vol. 42A, no. 2, pp. 32-44, 2013. [Online]. Available: Wiley Online Library, https://onlinelibrary.wiley.com. [Accessed Feb. 2, 2023].

[13]   T. Eo, Y. Jun, T. Kim, J. Jang, H. Lee, and D. Hwang, "KIKI-net: cross-domain convolutional neural networks for reconstructing undersampled magnetic resonance images," *Magn Reson Med,* vol. 80, pp. 2188-2201, 2018. [Online]. Available Wiley Online Library, https://onlinelibrary.wiley.com. [Accessed Jan. 30, 2023].

[14]   IBM, "Convolutional Neural Networks." IBM. https://www.ibm.com/topics/convolutional-neural-networks. [Accessed June 1, 2023].

[15]   Aphex34, "typical CNN architecture," Wikimedia Commons. 2015. https://commons.wikimedia.org/wiki/File:Typical_cnn.png. [Accessed June 1, 2023].

[16]   O. Ronneberger, P. Fischer, and T. Brox, "U-Net Convolutional Networks for Biomedical Segmentation," 2015. [Online serial]. Available: https://arxiv.org/abs/1505.04597. [Accessed Feb. 7, 2023].

[17]   C.M. Sandino, N. Dixit, J.Y. Cheng, and S.S. Vasanawala, "Deep convolutional neural networks for accelerated dynamic magnetic resonance imaging," 2017. [Online serial]. Available: http://cs231n.stanford.edu/reports/2017/pdfs/513.pdf. [Accessed May 14, 2023].

[18]   F. Knoll, P.M. Johnson, D.K. Sodickson, M.P. Recht, and Y.W. Lui, "NYU fastMRI Dataset: Brain MRI," *NYU Langone Health: fastMRI Dataset*, 2020. Available: https://fastmri.med.nyu.edu. [Accessed May 24, 2023].

[19]   F. Knoll et al., "fastMRI: A Publically Available Raw k-space and DICOM Dataset of Knee Images for Accelerated MR Image Reconstruction Using Machine Learning," *Radiology: Artificial Intelligence*, vol. 2, no. 1, 2020. [Online]. Available: RSNA, https://www.rsna.org. [Accessed May 24, 2023].

[20]   V. Ghodarti et al., "MR image reconstruction using deep learning: evaluation of network structure and loss functions," *Quant Imaging Med Surg*, vol. 9, no. 9, pp.1516-1527, 2019. [Online]. Available: QIMS, https://qims.amegroups.com. [Accessed May 14, 2023].

[21]   J. Zbontar et al., "fastMRI: An Open Dataset and Benchmarks for Accelerated MRI," 2018. [Online serial]. Available: https://arxiv.org/abs/1811.08839. [Accessed May 15, 2023].

[22]   T. Du, H. Zhang, Y. Li, H.K. Song, and Y. Fan, "Adaptive convolutional neural networks for k-space data interpolation in fast magnetic resonance imaging," 2020. [Online serial]. Available: https://arxiv.org/abs/2006.01385. [Accessed Jan. 30, 2023].

[23]   L. Xu, J. Xu, Q. Zheng, J. Yuan, and J. Liu, "A miniature U-net for *k*-space-based parallel magnetic resonance imaging reconstruction with a mixed loss function," *Quant Imaging Med Surg,* vol. 12, no. 9, pp. 4390-4401, 2022. [Online]. Available PubMed Central, https://www.ncbi.nlm.nih.gov/pmc/. [Accessed Feb. 7, 2023].

[24] Y. Han, L. Sunwoo, and J.C. Ye, "*k-space* Deep Learning for Accelerated MRI," *IEEE Transactions on Medical Imaging*, vol. 39, no. 2, pp. 377-386, 2020. [Online]. Available: IEEE Xplore, https://ieeexplore.ieee.org/Xplore/home.jsp. [Accessed Feb. 7, 2023].

[25] D.C. Preston, "Magnetic Resonance Imaging (MRI) of the Brain and Spine: Basics." Case Western Reserve University: Department of Neurology. 2016. https://case.edu/med/neurology/NR/MRI%20Basics.htm. [Accessed May 30, 2023].

[26] R. Bakshi, et al., "Fluid-Attenuated Inversion-Recovery MR Imaging in Acute and Subacute Cerebral Intraventricular Hemorrhage," *American Journal of Neuroradiology*, vol. 20, no. 4, 1999. [Online]. Available: NCBI-NIH, https://www.ncbi.nlm.nih.gov. [Accessed May 29, 2023].

[27] Z. Wang, A.C. Bovik, H.R. Sheikh, and E.P. Simoncelli, "Image quality assessment: from error visibility to structural similarity," *IEEE Transactions on Image Processing*, vol. 13, no. 4, pp. 600-612, 2004. [Online]. Available: IEEE Xplore, https://ieeexplore.ieee.org/Xplore/home.jsp. [Accessed May 27, 2023].

[28] J. Liu, Y. Sun, C. Eldeniz, W. Gan, H. An, and U.S. Kamilov, "RARE: Image Reconstruction using Deep Priors Learned without Groundtruth," 2020. [Online serial]. Available: https://arxiv.org/pdf/1912.05854. [Accessed June 21, 2023].

[29] U.S. Kamilov, C.A. Bouman, G.T. Buzzard, and B. Wohlberg, "Plug-and-Play Methods for Integrating Physical and Learned Models in Computational Imaging," 2022. [Online serial]. Available: https://arxiv.org/abs/2203.17061. [Accessed June 21, 2023].